Deuteron and proton magnetic resonance in amorphous silicon

D. J. Leopold,* Peter A. Fedders, and R. E. Norberg
Department of Physics, Washington University, St. Louis, Missouri 63130

J. B. Boyce and J. C. Knights
Xerox Palo Alto Research Center, Palo Alto, California 94304
(Received 19 October 1984)

Deuteron and proton NMR measurements have been made on a series of plasma-deposited *a*-Si:D,H samples. DMR line shapes show three components: a resolved quadrupolar doublet associated with D bonded to Si well removed from microvoids, a wide quadrupole-broadened central line associated with D located near to and on the surfaces of microvoids, and a sharp temperature-dependent feature associated with molecular D_2 in the larger voids. Dipolar T_2 decays show two components for both protons and deuterons. There is no strong correspondence between the dipolar broad and narrow lines and the two quadrupolar resonance components observed for bonded D. T_1(H) and T_1(D) show components associated with spin diffusion to effectively dilute H_2 and D_2 relaxation centers located in microvoids. SiD_4 and SiH_4 starting gases produce similar amounts of D_2 and H_2 under comparable deposition conditions. Two samples show a strong apparently electronic carrier-related nuclear-spin-lattice relaxation contribution near room temperature.

I. INTRODUCTION

Deuteron and proton NMR in *a*-Si:D,H provide a combination of perspectives about the microstructure of the material. Results previously reported[1] were obtained in a single, probably atypical, sample. The present work describes proton magnetic resonance and deuteron magnetic resonance (DMR) measurements on five plasma-deposited amorphous silicon samples prepared under varied conditions of starting gas mixture, rf power density, and substrate temperature. The DMR line shapes show three distinct components. A temperature-independent sharp DMR resolved doublet (RD) has the 66-kHz splitting reported[1,2] earlier and characteristic of a Si—D bonded configuration. All of the samples also show a temperature-independent quadrupole-broadened central line (BC), with clear broad peaks near the doublet singularities and a full width at half maximum (FWHM) slightly smaller than the splitting of the resolved doublet. In some samples there is a narrow central (NC) DMR component which arises from D_2 in the voids and shows continuous motional narrowing over the full temperature range investigated, from 4.2 to 300 K. The temperature dependence of the quadrupolar T_2 can be described[1] as an exponential process with two activation energies or, alternatively, by a power-law variation T^{δ} with $\delta \simeq 0.6$.

Dipolar spin-spin T_2 relaxation times for deuterons were measured using a quadrupole echo pulse sequence. The observed two-component dipolar decay of the quadrupole echo amplitude is compared with two-component dipolar rates observed for proton free-induction decays in the same samples. The comparison indicates that proton broadening of the deuteron resonance is effectively narrowed, and the H and D are located randomly in accord with the isotopic abundances.

Spin-lattice relaxation times for protons and the relaxation for two of the deuteron components show a low-temperature T_1 minimum (between 25 and 55 K) which reflects relaxation to fast-relaxing effectively dilute[3] molecular H_2 and D_2 impurities trapped in the films. Analyses of the T_1 minima yield temperature variations of the molecular electronic relaxation rates over 4 orders of magnitude for H_2 and D_2. These rates vary by an order of magnitude among the five *a*-Si samples studied. The H_2 and D_2 responsible for the H and D relaxation differ significantly[3] from the higher concentration H_2 reported from calorimetric[4–6] and infrared[7] measurements.

II. EXPERIMENTAL

Two broad-band pulsed NMR spectrometers described previously[1] were used to measure proton and deuteron relaxation times and line shapes from 4.2 to 450 K at several Larmor frequencies for five amorphous silicon samples plasma deposited from 100% SiH_4, 5% SiH_4/D_2, and 5% SiD_4/Ar gas mixtures. Thin film samples were deposited on both the grounded anode and ungrounded rf cathode using a plasma system described by Street, Knights, and Biegelsen.[8]

The samples were deposited on 2-in.-diam aluminum foil with typical rf power levels ranging from 2 to 20 W, corresponding to power densities of 0.1 to 1.0 W per square centimeter. The aluminum-foil backing was etched away with dilute HCl and the remaining 50—100-mg thin-film amorphous silicon flakes were placed in proton-free sample containers. Table I lists the preparation conditions for the five plasma-deposited samples studied along with the resulting proton and deuteron concentrations determined from calibrated NMR spin count comparisons with H_2O and D_2O. Also listed are lineshape fractions and H_2 and D_2 concentrations to be discussed later.

TABLE I. Sample preparation conditions and resulting H and D concentrations determined by NMR spin counts.

Sample	I	II	III	IV	V
Gas mixture	5% SiH_4/D_2		100% SiH_4	5% SiD_4/Ar	
Substrate temperature (°C)	25	25	230	25	230
Substrate	cathode	cathode	anode	cathode	anode
rf power (W)	18	2	2	15	15
$[n(H)+n(D)]$ at. %	31	23.3	10.9	17.0	11.7
$n(H)$ (at. %)	7	12.8	10.9	3.6	1.4
Broad	4	9.5	6.7	1.7	0.84
Narrow	3	3.3	4.2	1.9	0.56
$n(D)$ (at. %)	24	10.5		13.4	10.3
Resolved doublet (RD)	20	7.0		10.7	8.2
Broad central (BC)	1	3.5		2.7	2.1
$n(D_2)$ (at. %)					
Narrow central (NC)	1.5			<0.05	0.05
Effectively dilute relaxation centers					
$n(H_2)$ (ppm)	7.6	120	700	<0.2	<0.2
$n(D_2)$ (ppm)	670	?		5.9	3.8

We shall follow a convention of describing sample preparation conditions by the sequence: gas mixture, substrate temperature, deposition electrode, rf power. Reference 1 described proton and deuteron NMR measurements in sample I (5% SiH_4/D_2, 25 °C,*C*,18 W), which contained rather large amounts of D and relaxation-center D_2, with much of the D_2 presumably coming from the D_2 in the original gas mixture. In order to examine this question, two samples were prepared from a supposedly predeuterated mixture of 5% SiD_4 and 95% argon: sample IV (25 °C,*C*,15 W) and sample V (230 °C,*A*,15 W). Our calibrated NMR measurements show 3.6 and 1.5 at. % H, respectively, in samples IV and V and the starting gas mixture thus contained a small, but useful, hydrogen impurity. Sample II (5% SiH_4/D_2,25°C,2 W) was prepared at significantly lower rf power and deposition rate than those employed for sample I. Sample III (100% SiH_4,230 °C,*A*,2 W) was prepared from SiH_4 alone and deposited at low rf power on a heated substrate.

Spin-lattice relaxation times were measured using both an inversion recovery (180°-τ-90°) two pulse sequence and a repetition rate (180°-τ-90°-τ-90°-$\cdots$) saturation method. Deuteron resonance line shapes were obtained from Fourier transforms of quadrupole echoes generated using a (90°-τ-$90°_{90°}$) pulse sequence. Fourier-transform deuteron-magnetic-resonance—quadrupole echo (FTDMR-QE) line shapes were obtained by transforming the quadrupole echo starting at its peak at time 2τ. These 1024 point digital transforms were performed after averaging typically 100 sweeps to improve the signal-to-noise ratio.

Dipolar spin-spin T_2 relaxation times for deuterons were measured from the dependence of the quadrupole echo amplitude on the pulse time separation and then compared with proton free-induction-decay time constants. The echo amplitude decay envelope generated by varying τ reflects dipolar interactions which would determine the deuteron free-induction decay if the quadrupole interactions were absent and the magnet inhomogeneity was negligible.

III. RESULTS AND ANALYSES

A. Deuteron line shapes

The work reported in Ref. 1 described deuteron and proton NMR in sample I. Some of those previous results are summarized here for comparison with the other samples. Figure 1 shows 30-MHz FTDMR-QE line shapes for sample I at 4.2 and 39 K. The sweep width is 200 kHz and the full separation between the main peaks of the Pake doublet is 66 ± 1 kHz. The narrow central (NC) D_2 component of the resonance line shows motional narrowing and corresponds to 1.5 at. % D_2 and the resolved doublet and a broad central component, to 20 and 1 at. % D, respectively. The doublet component has a T_1 some 200 times longer than that of the narrow central D_2 line, which is relaxed by effectively dilute molecular p-D_2 relaxation centers. Sample I has the largest amount of D_2 of the samples described here.

The FTDMR line shape in Fig. 1, and all the other resonance line shapes presented here, are artificially symmetrized for visual presentation in the figures. Only one rf phase was detected and the FT shape functions necessarily are symmetric.

The 66-kHz doublet component in Fig. 1 was identified as arising from the electric field gradient associated with a bond to a single nearby silicon atom. The line shape corresponds to a powder-averaged resonance for an electric field gradient (efg) with very small, or zero, asymmetry parameter η (that is for an axial efg). The peak separation corresponds[1] to a deuteron quadrupole coupling constant

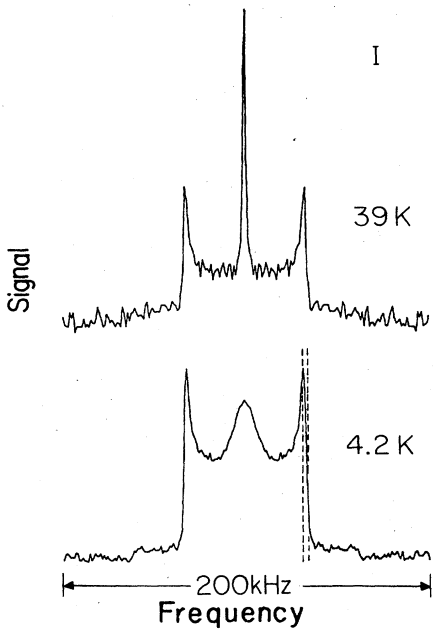

FIG. 1. Fourier transforms of 30.0-MHz deuteron 90°-τ-90°$_{90°}$ quadrupole echoes at 39 and 4.2 K for sample I. The resonance doublet has a full width splitting between the main peaks of 66±1 kHz. Also visible is a narrow component which arises from D_2 in microvoids and which broadens with reduced temperature. The vertical dashed lines correspond to ir stretching-mode absorptions, converted to quadrupole splittings.

$$\nu_q = \frac{eqQ}{h} = 88 \pm 1.3 \text{ kHz} , \quad (1)$$

which implies an efg at the deuterons corresponding to

$$q = (2.13 \pm 0.02) \times 10^5 \text{ dyn/cm} . \quad (2)$$

In diatomic molecules it has been shown[9] that (in atomic units) the stretching force constant is 1.127 times the field gradient at the deuteron. Such a relationship, applied to the a-Si result, Eq. (2), yields the stretching force constant

$$k = (2.40 \pm 0.02) \times 10^5 \text{ dyn/cm} \quad (3)$$

and an ir stretching-mode SiH spectrum at 2050±15 cm^{-1}. Infrared-absorption measurements[10] on a-Si:H samples deposited on room-temperature substrates have exhibited stretching-mode absorptions at reduced wave numbers between 2000 and 2200 cm^{-1}. For deuterated samples the stretching mode was shifted down to near 1460 cm^{-1}. The absorptions have been identified with structures SiH, SiH_2, $(SiH_2)_n$, and SiH_3. The vertical dashed lines in Fig. 1 correspond to two of these ir features to be discussed subsequently.

Figure 2 shows the 4.2-K FTDMR-QE spectrum for sample IA (not tabulated in Table I). The pulse separation was 400 μsec for the echo sequence. Sample IA (5% SiH_4/D_2,25 °C,A,18 W) was deposited on the ungrounded rf electrode in the same deposition which produced sample I. Sample IA has relatively less of the narrow central feature, compared to the doublet, than does sample I. The IA doublet splitting is the same as observed for sample I (and indeed for all samples described in the present paper).

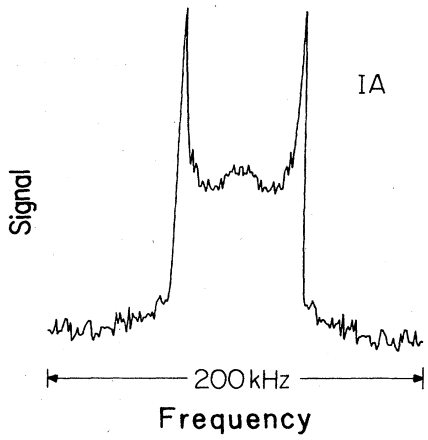

FIG. 2. Fourier transform of 30.0-MHz deuteron 90°-τ-90°$_{90°}$ quadrupole echo at 4.2 K for anode sample IA. The resonance doublet has a full width splitting between the main peaks of 66±1 kHz.

Figure 3 shows 5-K FTDMR-QE spectra for samples II and IV (Table I). Again the same temperature-independent axial efg Pake doublet appears in these spectra. There is more of the relatively broad central feature in the sample II resonance than in that for sample IV. In sample II the central feature has enough amplitude to obscure the limiting shoulders of the otherwise well-defined Pake doublet. There is a small amount of the narrow cen-

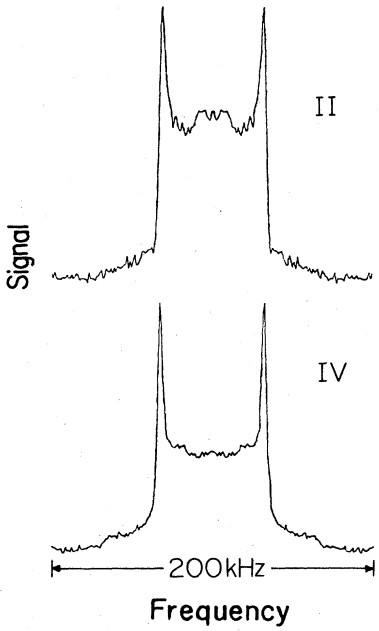

FIG. 3. Fourier transforms of deuteron 90°-τ-90°$_{90°}$ quadrupole echoes for samples II and IV at 5 K. The same doublet splitting of 66 kHz is observed for both samples. Sample II shows a larger central feature than does sample IV.

tral component in sample IV, but a DMR spectrum for sample II at 43 K indicates that sample II contains no appreciable amount of the motionally narrowed component shown in Fig. 1 for sample I.

Figure 4 shows FTDMR-QE spectra for sample V at three temperatures: 14, 23, and 33 K. The sharp doublet persists and the central sharp line is seen to motionally narrow between 14 and 33 K. The temperature variation of T_2 for the small central sharp line agrees with that observed (Fig. 1) and reported[1] for sample I. We believe that this narrow central line arises from molecular D_2 in the microvoids.

The third component of the DMR line is particularly clear in Fig. 4. There is a broad temperature-independent central line, observable also in the other samples (Table I). The smooth curve drawn on the 23-K spectrum in Fig. 4 is a Pake doublet fitted to the signal amplitude of the shoulders at twice the frequency of the sharp peaks. The dashed line shows, on a vertically-expanded scale, the difference spectrum between the smoothed 23-K data and the fitted Pake doublet. The difference spectrum is a bell-shaped curve with a full width at half maximum (FWHM) only slightly less than the 66-kHz doublet splitting. The broad side peaks in the difference spectrum have a long T_1, and probably belong with the doublet component, and represent a distribution of the observed silicon-deuteron local configurations. The broad central component corresponds in sample V to about one-quarter of the spin count of the resolved doublet. The T_1 of the broad central component is significantly less than that of the resolved doublet at intermediate temperatures between 10 and 100 K. Discussion of the probable structural identifications of the three quadrupole line-shape components is deferred to a later section.

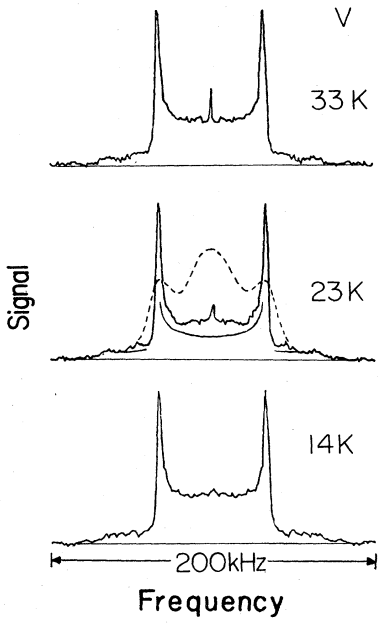

FIG. 4. Fourier transforms of deuteron $90°$-τ-$90°_{90°}$ quadrupole echoes at 33, 23, and 14 K for sample V. The resonance doublet has a full width splitting between the main peaks of 66 kHz. A small component at the center arises from molecular D_2 and shows motional narrowing. The solid curve shows a portion of a Pake doublet fitted to the 23-K data. The dashed line shows (on an enlarged vertical scale) the broad central line which is the difference between the 23-K data and the Pake doublet (and excluding the narrow central component).

Figure 5 shows a portion of the infrared spectrum observed for sample V. The stretching-mode absorptions for SiH ($\sim$2000 cm^{-1}) and SiD ($\sim$1460 to 1500 cm^{-1}) are prominent features. The full spectrum of sample V (and others) also shows scissors mode absorptions corresponding to SiHD and SiD_2 configurations. The vertical mark indicates the 1460 ± 10-cm^{-1} wave-number range corresponding [Eq. (3)] to the observed DMR resolved quadrupolar doublet splitting (Fig. 4) of 66 ± 1 kHz.

A comparison of the FTDMR spectra (Figs. 1—4 and Table I) is instructive. Proceeding from sample IV to V indicates that changing from a 25 °C cathode to a 230 °C anode substrate produces 20% decreases in the DMR resolved doublet (RD) and broad central (BC) fractions and a small, but significant increase in the temperature-dependent narrow feature. A reduction of deposition rate (rf power density, examined in a comparison of samples I and II) eliminates the narrow central (NC) line, reduces the doublet (RD), and increases the broad central (BC) resonance. The lower power density is accompanied by an increase in the n(H) from SiH_4, but a decrease in the n(D) from the D_2 starting gas. A comparison of samples I and IV shows DMR doublets and broad central (BC) lines essentially unchanged, but a reduction of the narrow component by a factor of more than 30. Apparently most of the narrow central fraction (NC) in sample I is associated with the fact that the deuterated starting gas was D_2 and that the deposition was rapid.

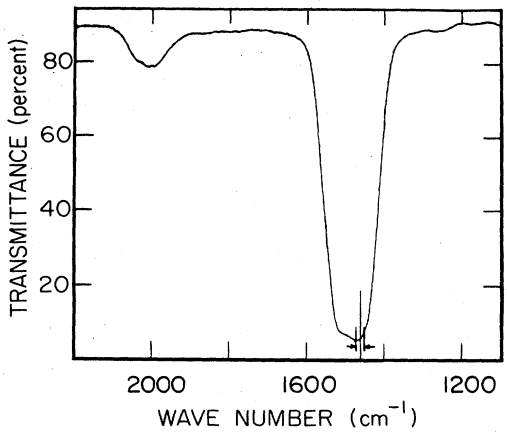

FIG. 5. Infrared spectrum for sample V showing stretching-mode absorptions for strongly bound deuterons and protons in the amorphous silicon film. The stretching frequency estimated from the tightly bound deuteron doublet splitting of 66 kHz is indicated by the vertical mark at 1460 ± 10 cm^{-1}.

B. Transverse relaxation

Typical proton free-induction decays show a two-component dipolar structure in almost all a-Si:H samples.[11,12] From such behavior two distinct clustered hydrogen phases are inferred to exist in the material. The deuteron free-induction decay following a 90° pulse reflects primarily an inhomogeneous quadrupole broadening of the resonance line shape resulting from static electric field gradients present at the deuteron sites. Some of the transverse dephasing of the deuteron free-induction decay can be time reversed by applying a $90°$-τ-$90°_{90°}$ quadrupole echo pulse sequence. The echo formed at time 2τ has a shape similar to the free-induction decay, but with a reduced amplitude which depends on the pulse separation τ. By plotting the quadrupole echo amplitude as a function of 2τ one obtains a decay envelope which reflects the dipolar spin-spin interaction.

Figures 6 and 7 show the results of such measurements on sample II at 5 K. The total deuteron and proton concentrations were found to be 10.5 and 12.8 at. %, respectively. The two-component structure for the deuteron quadrupole echo amplitude decay is shown in Fig. 6. An optimized fit to the data is found to yield (for signal percent components)

$$A(t)=53\exp[-t/(0.44\ \text{msec})] +47\exp[-t/(2.43\ \text{msec})]\ . \quad (4)$$

This double exponential fit to the deuteron quadrupole echo envelope corresponds to narrow and broad Lorentzian frequency spectra with full widths at half maximum (FWHM) 130 and 720 Hz.

The corresponding proton free-induction decay for sample II is shown in Fig. 7. The data have been corrected for a magnet inhomogeneity of 1.4 kHz (FWHM). Here a double exponential fit yields

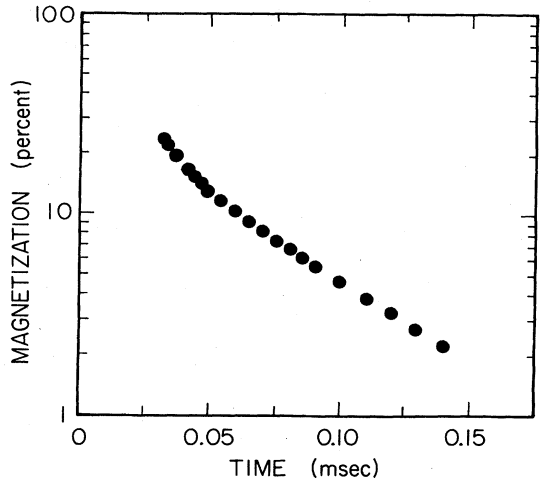

FIG. 7. The 30-MHz proton free-induction decay for sample II at 5 K. The data have been corrected for a magnet inhomogeneity characterized by $T_2^*(\mathrm{H})=230$ μsec. An optimized fit to the decay is $74e^{-t/0.016\ \text{msec}}+26e^{-t/0.069\ \text{msec}}$.

$$A(t)=74\exp[-t/(0.016\ \text{msec})] +26\exp[-t/(0.069\ \text{msec})]\ . \quad (5)$$

If the faster decay component is fitted with a Gaussian, then its relative amplitude is reduced to about 60%.

The proton decay times are shorter than those for the deuterons because of the larger gyromagnetic ratio for protons. The proton FWHM linewidths are 20 and 4.6 kHz. These are proton linewidths corrected for the 1400-Hz proton FWHM associated with the field inhomogeneity of solenoid over the a-Si sample. Both the proton and deuteron decay envelopes were found to be independent of temperature up to at least 300 K.

Figure 8 shows 30.0-MHz deuteron quadrupole echo

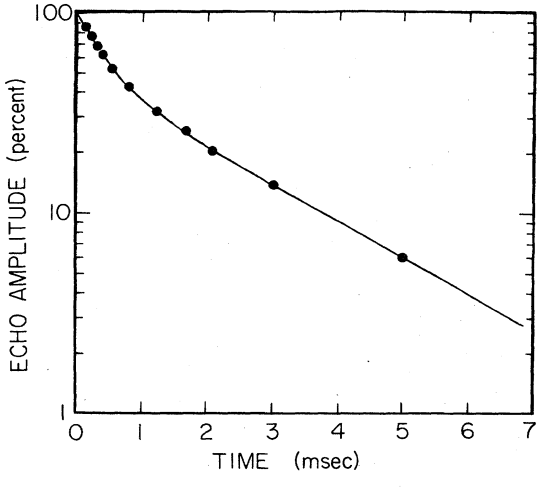

FIG. 6. The deuteron quadrupole echo envelope decay at 30.0 MHz for sample II at 5 K shows a double exponential structure. An optimized fit shown by the curved line is $53e^{-t/0.44\ \text{msec}}+47e^{-t/2.43\ \text{msec}}$.

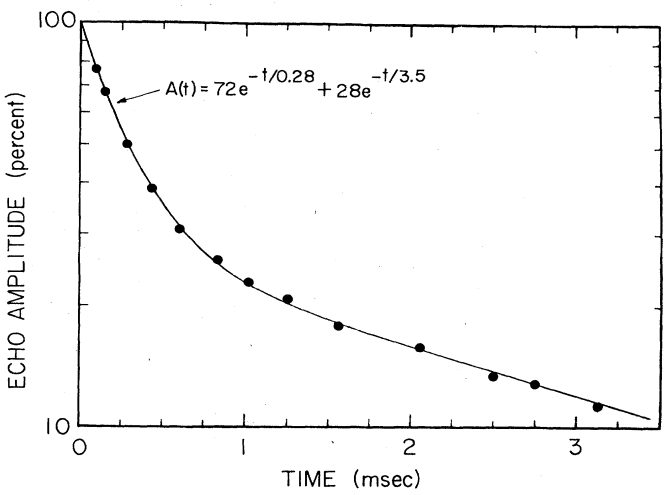

FIG. 8. The deuteron quadrupole echo envelope decay at 30.0 MHz for sample V at 5.7 shows a double exponential structure. An optimized fit shown by the curved line is $72e^{-t/0.28\ \text{msec}}+28e^{-t/3.50\ \text{msec}}$.

amplitude data obtained at 5.7 K for sample V. The total deuteron concentration for this sample was found to be 10.4 at.% with a small 1.4-at.% proton signal arising from an impure gas used in the plasma discharge. Again a two-component deuteron echo amplitude decay is observed with

$$A(t)=72e^{-t/(0.28\ \text{msec})}+28e^{-t/(3.50\ \text{msec})}. \quad (6)$$

These dipolar decay results, together with those for the 300-K proton FID in sample V, are summarized in Table II. The proton linewidths have been corrected for a magnet inhomogeneity of 1.4 kHz (FWHM). The widths observed for the broad and narrow proton resonance components are typical of those reported[11] for hydrogen in plasma-deposited *a*-Si. Such linewidths have been interpreted[11,12] to reflect proton dipolar broadening in spatially separated phases, both clustered, but with significantly more hydrogen clustering in the broad-line fraction. In Table II the broad to narrow linewidth ratios are 2 to 5 times larger than the corresponding fraction ratios and reflect the larger degree of H and D clustering in the broad-line fractions.

In sample V, with only 1.4 at.% H present, there still are 60% broad-line and 40% narrow-line H fractions present with standard clustering reflected by proton NMR widths of 24 and 3.1 kHz, respectively. These are comparable to widths observed in samples with 10 times more H present, so the proton linewidths do not show a significant effect of deuteron dilution.[11] The 60/40 division of H indicates that both H and D go into the deposited film in a similar manner, since for *a*-Si:H samples below 3 at.% H, it is usual to find only the less-clustered narrow-line $\delta\nu_H$ component. The total hydrogen content of sample V is, however, 11.7 at.% and both H and D NMR reflect the presence of both clustered phases.

There is a substantial consistency in the dipolar widths listed in Table II. If the H and D isotopes substitute randomly in the *a*-Si samples, then the H-D dipolar interaction (for $f_H=f_D$) will contribute only 1.4% of the proton linewidths. The proton dipolar FID-based FWHM δ_H widths then primarily reflect like-spin broadening. The situation is reversed for deuteron widths δ_D. Here an assumption of similar H and D spatial distributions implies that the protons contribute 93% of the deuteron dipolar widths. However, the observed FTDMR-QE δ_D are larger for sample V (1.4 at.% H) than for sample II (12.8 at.% H).

If the proton FID and the deuteron QE envelopes both decay with times limited by the usual dipolar interaction with protons, then in an isotopically uniform sample the ratio of widths is

$$\frac{\delta\nu_H}{\delta\nu_D}=\left[\frac{\gamma_H^4 I_H(I_H+1)}{\frac{4}{9}\gamma_D^2\gamma_H^2 I_H(I_H+1)}\right]^{1/2}=9.77\ . \quad (7)$$

If H-D and D-D interactions are included the ratio becomes 9.27 (assuming equal local concentrations of H and D). These ratios are significantly smaller than all four δ_H/δ_D ratios given in Table II. The observed ratios range from 22 to 35, with an average slightly less than 30.

However, for similar local abundances of protons and deuterons, the H-H dipolar interaction is so large (24 kHz) that the proton dipolar flip flops associated with $I_{j+}I_{k-}$ are much faster (18 kHz) than the D-H dipolar interaction width (2.4 kHz). Thus the proton *z* fields seen by the deuterons are effectively narrowed[13] and only the D-D dipolar *z*-component interaction damps the DMR-QE envelope. It is as if the deuteron quadrupole echo envelope reflected local predeuteration in which case the anticipated[14] ratio is

TABLE II. Transverse dipolar relaxation in two *a*-Si samples.

	II 5% SiH_4/95% D_2 25°C, 2 W, cathode 12.8 at.% H, 10.5 at.% D		V 5% SiD_4/95% Ar 230°C, 15 W, anode 1.4 at.% H, 10.3 at.% D	
	Fast	Slow	Fast	Slow
H (FID)				
Relative f_H	0.74	0.26	0.60	0.40
f_H (at.%)	9.5	3.3	0.84	0.56
δ_H (kHz, FWHM)	20.0	4.6	23.7	3.12
F/S f_H ratio	2.9		1.5	
F/S δ_H ratio	4.3		7.6	
D (QE envelope)				
Relative f_D	0.53	0.47	0.72	0.28
f_D (at.%)	5.6	4.9	7.4	2.9
δ_D (Hz, FWHM)	720	130	1100	91
F/S f_D ratio	1.1		2.6	
F/S δ_D ratio	5.5		12	
δ_H/δ_D	28	35	22	34

$$\frac{\delta_H}{\delta_D}=\left[\frac{\gamma_H^4 I_H(I_H+1)}{\frac{5}{6}\gamma_D^4 I_D(I_D+1)}\right]^{1/2}=28.5\,, \tag{8}$$

in good agreement with the four results in Table II. The factor of $\frac{5}{6}$ enters for dipolar coupled D pairs with the same absolute quadrupolar coupling, $|\omega_q|$.

Local predeuteration is reasonable in sample V, where there is an order of magnitude more D than H. It is not reasonable in sample II, but there the D-H interaction is narrowed out. Thus the widths δ_H and δ_D and their ratios δ_H/δ_D indicate that the proton FID transverse decay rates are determined by H in both samples and that the QE envelope deuteron transverse decays reflect D-D couplings only.

The shape of the quadrupole echo changes as a function of pulse separation τ. Figure 9 shows a superposition of FTDMR-QE line shapes for sample IV at 6.3 K and at three-pulse separation intervals. The solid curve shows the FT line shape for the quadrupole echo at $2\tau=100$ μsec. The half-curve on the lower left-hand side shows the FT line shape for $2\tau=400$ μsec, and the half-curve on the lower right-hand side shows that for $2\tau=1200$ μsec. The FT lines each have been normalized to represent 96 averaged transients. The decay envelope of the sample-IV echoes is in reasonable agreement with the compound decay shown in Fig. 8 for sample V.

The spectrum obtained (Fig. 9) from the sample-IV quadrupole echo at $2\tau=100$ μsec shows a broader doublet distribution and a larger central quadrupolar component than do the spectra for echoes at 400 and 1200 μsec. The spectrum obtained with the smaller echo delay time contains signals from both the highly-clustered and the less-clustered deuteron fractions. However, in accordance with the evolution of the two-component dipolar decay of the DMR echo amplitude (Figs. 6 and 8), the FTDMR spectra obtained from echoes at long times 2τ include primarily signals from the less-clustered fraction and these are seen to correspond to a more-sharply-defined quadrupolar doublet. Observations in two samples indicate that the damping is independent of temperature between 4 and 50 K.

Figure 10 shows again the $2\tau=100$-μsec echo spectrum of Fig. 9. For comparison, the dashed line shows the smoothed difference spectrum between those for echoes at 100 and 1200 μsec in Fig. 9. The dashed line represents the spectrum of the more-rapidly-decaying fraction of the DMR echo envelope and is seen to correspond to a broad central peak with distributed features near the location of the doublet peaks in RD. The difference spectrum in fact bears a close resemblance to the temperature-independent broad central component deduced for sample V by subtracting a Pake doublet in Fig. 4. A similar central peak with side lobes results from a subtraction of a 66-kHz Pake doublet from the DMR spectra for all of the deuterated samples described in Sec. III A. The quadrupolar side lobes in the difference spectra probably belong with the resolved doublet fraction.

Nevertheless, comparison of Tables I and II shows that there is no correlation between the deuteron populations in the fast and slow dipolar decay (more and less clustered) components and the populations in the distribution of quadrupolar line shapes (resolved doublet and broad central). The quadrupolar line-shape fractions correspond to the spin-lattice relaxation components in the temperature region where there is a distinguishable more rapid D_2-related $T_{1\alpha}$(D). We conclude that the resolved doublet and broad central line-shape components each contain both more-clustered and less-clustered deuterons.

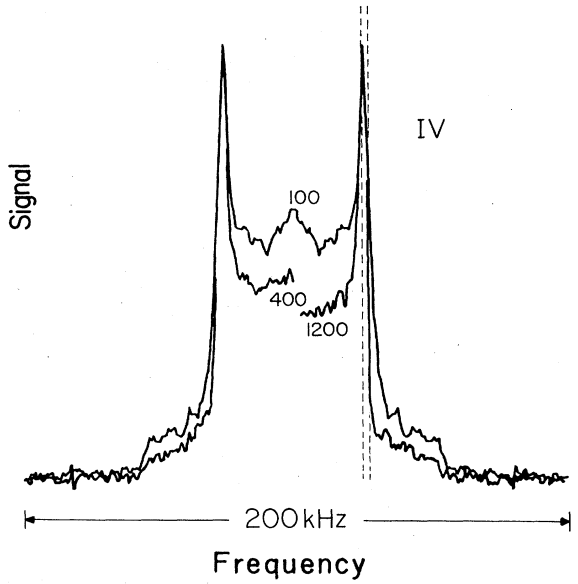

FIG. 9. Fourier transforms of 30.0-MHz deuteron 90°-τ-90°$_{90°}$ quadrupole echoes for different pulse spacings are shown for sample IV at 6.3 K. The Fourier-transform line obtained from the echo at $2\tau=100$ μsec shows a broader distribution of quadrupolar couplings than those obtained for the echoes at $2\tau=400$ and 1200 μsec. The doublet splitting between the main peaks is 66 kHz for all three transform resonance lines. The solid curve is for $2\tau=100$ μsec, the half-curve at the lower left is for $2\tau=400$ μsec, and that at the lower right is for 1200 μsec. The vertical dashed lines correspond to ir stretching-mode absorptions, converted to quadrupole splitting.

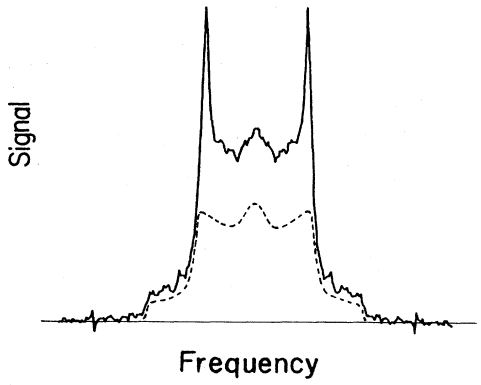

FIG. 10. The dashed line shows the smoothed difference spectrum between the Fig. 9 FTMDR-QE spectra for $2\tau=100$ μsec (shown again here) and 1200 μsec (sample IV, 6.3 K).

Figure 10 shows that there are more of the more-clustered rapidly-decaying deuterons in the quadrupolar broad central line, but the side bumps of the difference spectrum belong with the long T_1 resolved doublet fraction. Saturation T_1 runs have not shown residual beat patterns on the quadrupole echoes at rapid repetition rates.

It is our interpretation that the DMR doublet fraction RD corresponds principally to the binding configurations SiD and SiD_2. In most *a*-Si:H samples SiH is characterized[10] by an ir stretching-mode absorption at 2000 cm^{-1} and SiH_2 (and SiH in different environments) by an absorption at 2090 cm^{-1}. The corresponding deuteride stretching modes occur at wave numbers reduced by a factor of 1.37 (instead of the 1.39 anticipated from a primitive comparison of molecular reduced masses). These wave numbers correspond to (Sec. III A) $\eta=0$ quadrupolar Pake doublet singularities predicted (for SiH) to occur at 64.9 and 70.9 kHz, respectively. These are indicated by the dashed vertical lines in Figs. 1 and 9 for comparison with the line-shape data for samples I and IV. SiH_3 configurations correspond to stretching modes near 2140 cm^{-1} and SiD_3 quadrupolar singularities at 74.4 kHz, somewhat farther out in the wings of Fig. 9 than the SiD_2 line at 70.9 kHz.

The observed ir stretching-mode absorptions have overlapping spectra which extend from about 1950 to 2150 cm^{-1}. This range corresponds to a distribution of quadrupolar DMR splittings over an interval somewhat larger than twice the separation of the dashed lines in Figs. 1 and 9. The ir stretching modes in *a*-Si have wave numbers some 50 to 100 cm^{-1} smaller[10] than those in the corresponding molecules. The linear relationship between stretching frequency and force constant may differ for SiD and SiD_2. All of these effects are not likely to alter our identification of the resolved doublet DMR component RD with well-defined axial SiD and SiD_2 tightly-bonded species. Scissors-mode ir spectra are present even in the 230 °C substrate sample V.

C. Spin-lattice relaxation

1. *Relaxation by molecular hydrogen*

Most plasma-deposited *a*-Si:H films show a proton spin-lattice relaxation time minimum[15] between 25 and 55 K. A time $T_{1\alpha}(H)$ reflects relaxation[1,15] of bonded protons by spin diffusion to effectively dilute[3] rapidly-relaxing *o*-H_2 molecules. Below 120 K the *o*-H_2 molecules predominantly are in their $J=1$ rotational states. The relaxation-center *o*-H_2 are effectively dilute in that their electric quadrupole-quadrupole (EQQ) interactions are quenched[3] although H_2 occurs at large density[7] in the *a*-Si voids. In many samples there also is an additional longer proton relaxation time $T_{1\beta}(H)$,[16] which decreases slowly with increasing temperature. This additional relaxation probably is associated with dangling bonds and usually makes only a small contribution to the overall proton relaxation near the $T_1(H)$ minimum, but sometimes a more significant contribution at higher and lower temperatures. The observed proton relaxation rate then can be written

$$\frac{1}{T_1(H)}=\frac{1}{T_{1\alpha}(H)}+\frac{1}{T_{1\beta}(H)} . \tag{9}$$

We have reported[1] deuteron spin-lattice relaxation measurements for *a*-Si:D,H sample I. The nondoublet DMR component shows a $T_{1\alpha}$ minimum (near 25 K at 30 MHz) which arises from rapid spin diffusion to effectively dilute *p*-D_2 relaxation centers. The DMR doublet fraction shows much longer relaxation times and no observed low-temperature $T_1(D)$ minimum.

In their rotational ground states, both *o*-H_2 and *p*-D_2 have $I=1$ and $J=1$ and thus are described by similar relaxation analyses. The $I=0$, $J=0$, *p*-H_2, and *o*-D_2 components are ineffective as nuclear relaxation centers. The $I=2$ molecular *o*-D_2 fraction has long nuclear relaxation times in the $J=0$ state and need not be considered as relaxation centers in analyses of the $T_{1\alpha}(D)$ relaxation near the observed $T_1(D)$ minima. Above 80 K, the effects of higher rotational states, including those of both *o*-D_2 and *p*-D_2, must be included[17] in the analysis of $T_{1\alpha}(D)$. Similarly, above 120 K, higher J states of *o*-H_2 play an appreciable role[17] in determining $T_{1\alpha}(H)$.

Nuclear relaxation of effectively dilute H_2 or D_2 in a nonmagnetic solid depends on the magnitude and symmetry of static efg which may exist at the molecular sites. For large gradients with no symmetry (and a parameter $r=0$), the angular-averaged nuclear relaxation rate in *o*-H_2 or *p*-H_2 with $J=1$ is[18]

$$\frac{1}{T_1}=\tfrac{6}{5}\omega_d^2[F_2(\omega_0)+4F_2(2\omega_0)] . \tag{10}$$

Here $F_2(\omega)=\Gamma_2/(\Gamma_2^2+\omega^2)$ and Γ_2 is the decay rate (electronic molecular correlation frequency) for quadrupole $l=2$ correlation functions. The interaction frequencies ω_d are[19] $\omega_d(H_2)=3.624\times10^5$ sec^{-1} and $\omega_d(D_2)=1.588\times10^5$ sec^{-1}. In rare-gas solids and in many *a*-Si samples it is found that the molecular relaxation of dilute *o*-H_2 and *p*-D_2 above about 3 K can be described via a phonon-Raman process. It then is anticipated[20,21] that

$$\Gamma_2=CE^*(T^*)(T^*)^2 , \tag{11}$$

where $E^*(T^*)$ is the tabulated[20] Van Kranendonk function, T^* is a reduced temperature T/Θ_c, and Θ_c is a characteristic temperature.

The spin-lattice relaxation data near the observed T_1 minima for protons and deuterons bonded in *a*-Si will be fitted to expressions which include both rapid and bottleneck spin-diffusion terms:

$$T_{1\alpha}(H)=AT_1(H_2)+B , \tag{12}$$

$$T_{1\alpha}(D)=A'T_1(D_2)+B' . \tag{13}$$

The coefficient of the rapid spin-diffusion term is given by the ratio of spin heat capacities (assuming A and $A'\gg1$)

$$A=\frac{T_1(H)}{T_1(H_2)}=\frac{n(H)I(I+1)}{\frac{3}{4}n(H_2)S(S+1)} \tag{14}$$

and

$$A' = \frac{T_1(\mathrm{D})}{T_1(\mathrm{D}_2)} = \frac{n(\mathrm{D})I(I+1)}{\frac{1}{3}n(\mathrm{D}_2)S(S+1)} . \quad (15)$$

Here $n(\mathrm{H})$ and $n(\mathrm{D})$ are the concentrations of silicon-bonded protons and deuterons relaxing to effectively dilute molecular o-H_2 and p-D_2, respectively; $n(H_2)$ and $n(D_2)$ are the concentrations of these rapid nuclear relaxation components of molecular H_2 and D_2 trapped in the a-Si film; I is the nuclear spin of $\mathrm{H}(I=\frac{1}{2})$ or $\mathrm{D}(I=1)$; and S is the nuclear spin of o-H_2 and p-$D_2(S=1)$. We have here neglected the effects of higher J states near the T_1 minima and have taken the equilibrium room-temperature o-H_2 and p-D_2 fractions ($\frac{3}{4}$ and $\frac{1}{3}$, respectively).

The bottleneck relaxation rates can be described by[1,15]

$$\frac{1}{B} = (4\pi D_{\mathrm{H}} b_{\mathrm{H}})[\tfrac{3}{4}n(\mathrm{H}_2)] \quad (16)$$

and

$$\frac{1}{B'} = (4\pi D_{\mathrm{D}} b_{\mathrm{D}})[\tfrac{1}{3}n(\mathrm{D}_2)] . \quad (17)$$

Here the D_{H} and D_{D} are spin-diffusion coefficients and the b_{H} and b_{D} are the characteristic distance between H_2 (D_2) and its nearest H (D) neighbor.

Figure 11 summarizes the temperature variations of proton T_1(H) data for samples II and III. Both show low-temperature T_1(H) minima which arise from rapid spin diffusion to o-H_2. The inverted solid triangles show the 42.3-MHz T_1(H) reported[16] for a sputtered sample (Harvard No. 1) which was prepared so as to have no H_2 in the film. The Harvard sample shows the characteristic temperature variation of T_1(H) associated with relaxation by dangling bonds. A smooth curve fitted to these data provides the non-H_2-related term $T_{1\beta}$(H) which we use in Eq. (9) with the sample-III T_1(H) data (open triangles) of Fig. 11. The resulting $T_{1\alpha}$(H) are shown as open circles at the bottom of Fig. 12, together with the fitted curve for sample III (assuming dilute molecular o-H_2 in the presence of large efg with no symmetry, neglecting intermolecular EQQ interactions, and for a characteristic temperature $\Theta_c = 40$ K)

$$T_{1\alpha}(\mathrm{H}) = 78T_1(\mathrm{H}_2) + 0.22 \text{ sec} . \quad (18)$$

The proton T_1(H) data for sample II also shown in Fig. 11 require $T_{1\beta}$(H) times some 50% larger than the Harvard No. 1 data. The resulting H_2-related $T_{1\alpha}$(H) for sample II are shown as solid points at the top of Fig. 12, together with the two lines which represent a reasonable fit to the $T_{1\alpha}$(H) results for sample II at both 46 and 92 MHz,

$$T_{1\alpha}(\mathrm{H}) = 542T_1(\mathrm{H}_2) + 1.8 \text{ sec} . \quad (19)$$

Equations (18) and (19), combined with Eqs. (14) and (15), the n(H) listed in Table I, and taking $b_{\mathrm{H}} = 4\times10^{-8}$ cm, yield the following for sample II: $n(H_2) = 120$ ppm, $D_{\mathrm{H}} = 2.5\times10^{-13}$ cm^2/sec; and for sample III: $n(H_2) = 700$ ppm, $D_{\mathrm{H}} = 3.5\times10^{-13}$ cm^2 sec. These results and similar conclusions for the other samples are summarized in Table III.

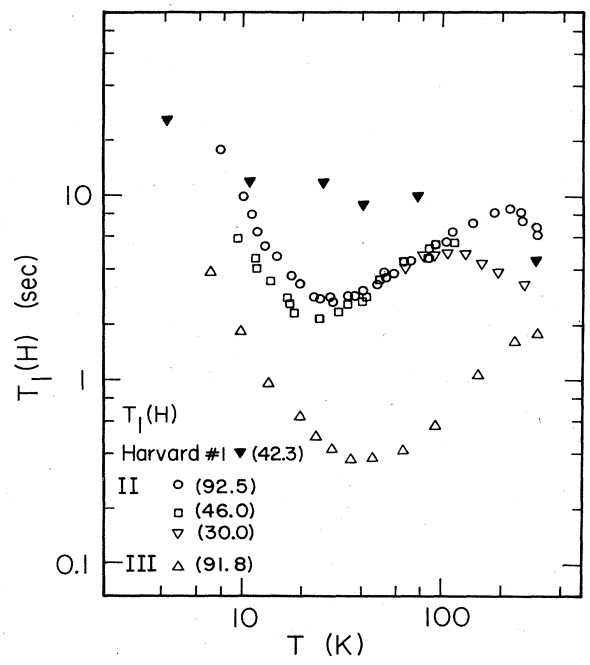

FIG. 11. Proton spin-lattice relaxation times T_1 for samples II and III. For comparison the solid triangles show T_1(H) reported (Ref. 16) for a sputtered sample which was prepared so as to have little or no H_2.

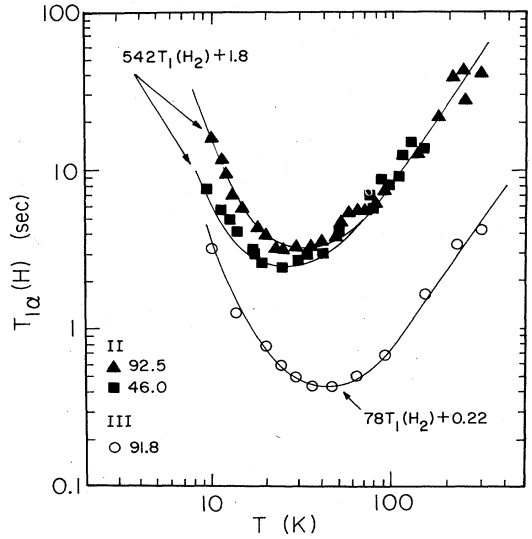

FIG. 12. Molecular-hydrogen-related $T_{1\alpha}$(H) data and corresponding fits are shown for samples II and III. The line drawn through the $T_{1\alpha}$(H) data of sample II is [$542T_1(H_2) + 1.8$ sec] and shows T_1 minima at 25 and 34 K for 46.0 and 92.5 MHz, respectively. The line drawn through the 91.8-MHz $T_{1\alpha}$(H) data for sample III is [$78T_1(H_2) + 0.22$ sec] and has a T_1 minimum at 43 K.

TABLE III. Molecular H_2- and D_2-related relaxation fits and corresponding results.

Sample	T_1 (D) (sec)	Central lines (BC) n(D) or (NC) $n(D_2)$ (at. %)	Effectively dilute relaxation centers $n(D_2)$ (ppm)	D_D (cm^2/sec)
I	$134T_1(D_2)+0.13$	1.5(D_2)	670	1.1×10^{-12}
IV	$13\,800T_1(D_2)+16$	2.7(D)	5.9	1.3×10^{-12}
V	$16\,500T_1(D_2)+64$	2.1(D)	3.8	4.9×10^{-13}
Sample	$T_{1\alpha}$(H) (sec)	n(H) (at. %)	$n(H_2)$ (ppm)	D_H (cm^2/sec)
I	$4590T_1(H_2)+0.25$	7.0	7.6	2.8×10^{-11}
II	$542T_1(H_2)+1.8$	12.8	120	2.5×10^{-13}
III	$78T_1(H_2)+0.22$	10.9	700	3.5×10^{-13}
IV		3.3	<0.2	
V		1.4	<0.2	

The proton relaxation time data for samples II and III in Fig. 12 fall somewhat below the T^2 fitted lines above 150 K. A more correct fitting procedure would employ the recently derived[17] full $J>1$ o-H_2 relaxation expressions. It has been pointed out[22] that because the T_1(H) times for sample III still are increasing with T at 300 K, the o-H_2 relaxation centers in this sample must experience static efg of low symmetry. The frequency dependence of the warm-sample T_1(H) for sample II (Fig. 11) above 100 K indicates the presence of a motional T_1(H) contribution. It may arise from proton diffusion or may be associated with a paramagnetic impurity, but it obscures any proton relaxation from $J>1$ o-H_2.

The fits of Eqs. (18) and (19) to the low-temperature T_1 data are imperfect, particularly so for Eq. (19) and sample II. We believe that the difficulty is associated with the presence of a distribution[3] of EQQ interactions between o-H_2 molecules and a corresponding distribution of molecular correlation frequencies which will be considered after relaxation results for all the samples have been discussed.

T_1(D) for the doublet component turned out to be similar in samples IV and V at 30 MHz. The doublet relaxation times are represented by open and solid circles at the top of Fig. 13. T_1(D) for the central component is shown as triangles (sample IV) and squares (sample V), also at the top of Fig. 13. There is a weak, but clear, central component, T_1(D) minimum in the data for sample IV (and a less-clear D_2-related contribution for sample V).

The broad central fraction deuteron T_1(D) results for sample IV can be analyzed by using the deuteron analog of Eq. (9) and taking the T_1(D) data for the sample-IV doublet to be $T_{1\beta}$(D). The resulting molecular-D_2-related $T_{1\alpha}$(D) are shown as solid triangles at the top of Fig. 14. A similar $T_{1\beta}$(D) subtraction procedure yields the $T_{1\alpha}$(D) for sample V indicated by solid diamonds at the top of Fig. 14. The solid lines through the limited $T_{1\alpha}$(D) data indicate the approximate fits of Eq. (13) for sample IV,

$$T_{1\alpha}(D)=13\,800T_1(D_2)+16 \text{ sec}, \quad (20)$$

and for sample V,

$$T_{1\alpha}(D)=16\,500T_1(D_2)+64 \text{ sec}. \quad (21)$$

Here we again have employed $\Theta_c=40$ K and assumed large static efg of no symmetry (with $r=0$) at the sites of

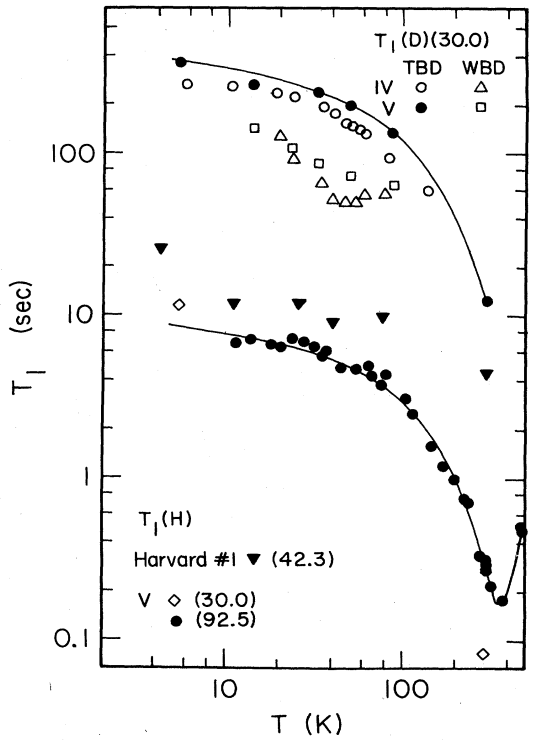

FIG. 13. Spin-lattice relaxation times T_1 for D at 30.0 MHz in samples IV and V are shown at the top of the figure. The open and solid circles are relaxation times associated with the tightly bound deuteron doublet. The open triangles and squares are relaxation times for the unsplit weakly bound deuteron fractions which show para-D_2-related relaxation minima. At the bottom of the figure are shown proton spin-lattice relaxation times T_1(H) at 30.0 and 92.5 MHz for sample V. The lines are drawn with a ratio 42.44.

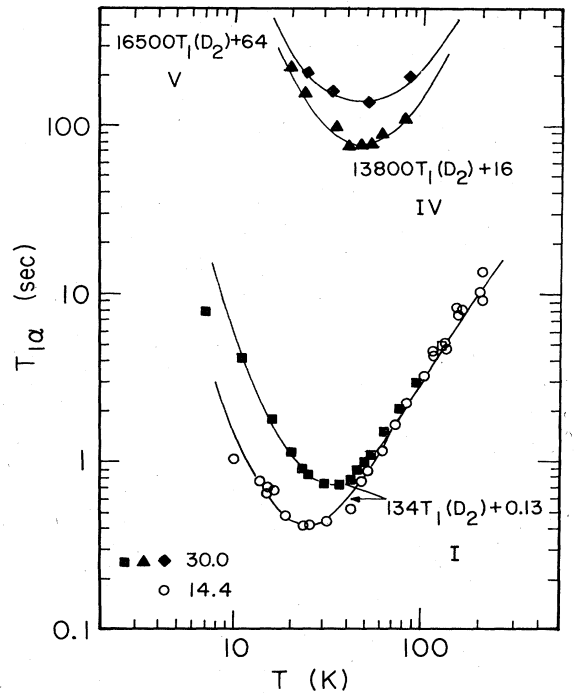

FIG. 14. Molecular-deuterium-related $T_{1\alpha}$(D) data and corresponding fits are shown for samples I, IV, and V. The line through the 30.0-MHz $T_{1\alpha}$(D) data of sample V is [16 500$T_1(D_2)$ + 64 sec] and has a T_1 minimum at 47 K. The corresponding line through the 30.0-MHz $T_{1\alpha}$(D) data of sample IV is [13 800$T_1(D_2)$ + 16 sec] and also has a T_1 minimum at 47 K. The 14.4 and 30.0-MHz $T_{1\alpha}(D_2)$ data for sample I are fitted by the [134$T_1(D_2)$ + 0.13 sec] lines shown at at the bottom of the figure.

the (assumed $J=1$) p-D_2. The $T_1(D_2)$ have been calculated for effectively isolated[3] p-D_2 molecules and a 30-MHz deuteron Larmor frequency. Θ_c, which describes the local phonon dynamics as it enters the Raman mechanism characterizing the p-D_2 molecular relaxation, has not yet been measured directly by observation of $T_1(D_2)$ for p-D_2 in a-Si or in rare-gas solids, but $\Theta_c=40$ K gave a reasonable fit to the previously reported and more extensive $T_{1\alpha}(D_2)$ data for sample I.

In the lower portion of Fig. 14 the circles and solid squares indicate for comparison the much more rapid $T_{1\alpha}(D_2)$ relaxation times for the NC void bulk D_2 component for sample I at 14.4 and 30.0 MHz. The lines drawn correspond to the fit of Eq. (13) in this case,

$$T_{1\alpha}(\text{bulk } D_2)=134T_1(D_2)+0.13 \text{ sec} . \quad (22)$$

Application of Eqs. (15) and (17) to the broad central component $T_{1\alpha}$(D) results for samples IV and V yield the parameters listed in Table III. Taking the NC component for sample I to be bulk (o-D_2+p-D_2), Eq. (15) must be modified to have a numerator $4n$(bulk D_2).

According to Eqs. (15) and (20), the rapid-term ratio $T_{1\alpha}D/T_1(D_2)$ is 13 800 for sample IV, and so $n(D)=4600n(D_2)$ for the relaxation center D_2 in this sample. The fast-relaxing deuteron signals were found to correspond to 25% of the observed DMR in samples IV and V, and so for IV (Table I) the broad central $n(D)=2.7\%$ and $n(D_2)=5.9\times10^{-6}$ (5.9 ppm). For an a-Si site number density of 5×10^{22} cm^{-3} this corresponds to $n(D_2)=2.9\times10^{17}$ cm^{-3} for sample IV. This is a concentration similar to that reported[1] for $n(H_2)$ (3.8×10^{17} cm^{-3}) in sample I, so the amounts of relaxation-center molecular H_2 formed from 5% SiH_4 and D_2 formed from 5% SiD_4 are similar for the two samples made on room-temperature cathode substrates at similar rf power levels.

A few $T_1(D)$ measurements were made on sample II. At 4.2 K $T_1(D)$ was very long (hundreds of seconds) and at 45 K two $T_1(D)$ components were observed. However, the shorter $T_1(D)$ at 45 K was about 50 sec, some 2 orders of magnitude longer than the fast $T_1(D)$ component in the companion sample I (Fig. 14), deposited at higher rf power density. Sample II does not have an appreciable narrowed central (NC) D_2 component (Table I and Fig. 3). Similar results were obtained for sample IA (Fig. 2). Apparently the molecular-D_2-related relaxation $T_{1\alpha}(D)$ process for the broad central (BC) component is significantly less efficient than that for the narrow central (NC) component.

Table III lists the fits of Eqs. (12) and (13) to the spin-lattice relaxation time minima in the five a-Si samples studied. The table also summarizes the molecular $n(H_2)$ and $n(D_2)$ concentrations determined from NC component spin counts and from the rapid spin-diffusion relaxation fits using the spin heat capacities, Eqs. (14) and (15), and the measured total concentrations (also listed in Table I) n(H) for the total protons and n(D) for the non-doublet central DMR fractions.

Samples IV and V did not show low-temperature proton T_1(H) minima. From this it follows that the concentrations of molecular H_2 in these two samples were less than 0.2 ppm and that the large deuterium dilution may have interfered[11] with proton spin diffusion, despite the standard proton linewidths observed (Table II). It is evident that a few ppm of o-H_2 and p-D_2 molecules can dominate the bulk proton and deuteron relaxation over a significant temperature interval in a-Si.

The results in Table III have been calculated on the assumption that the effectively dilute H_2 and D_2 relaxation centers are located at sites with large static electric field gradients (efg) of no symmetry. If the efg have axial symmetry then the tabulated molecular relaxation center concentrations are too large by a factor of 2 and the spin-diffusion coefficients are too small by a factor of 2. However, the temperature variation of the relaxation times observed near room temperature for samples II and III indicates[22] that the efg in these samples have symmetries much less than axial and the no-symmetry approximation probably is valid. The conclusion arises from consideration of the effects[17] of higher J states on the relaxation of H_2 and D_2 above 80 K.

2. *Molecular relaxation rates*

From each $T_{1\alpha}$(H) and $T_{1\alpha}$(D) data point a molecular correlation frequency Γ_2 can be calculated for the effectively dilute o-H_2 and p-D_2 relaxation center molecules in the various a-Si samples. For static efg of no symmetry

the individual T_1 results are inserted into Eq. (10) and a solution Γ_2 is found. Figure 15 shows the resulting Γ_2 as a function of temperature for samples I, II, III, and IV. As expected, the Γ_2 results for sample I are the same[1] (below 100 K) for both H_2 and D_2.

The curved lines represent Γ_2 reported[23] for o-H_2 in solid neon and argon. The lines indicate the temperature dependence given by Eq. (11) with $\Theta_c = 40$ K, efg of no symmetry, and the temperatures of the $T_{1\alpha}$(H) minima taken to be those observed in neon and argon. The Van Kranendonk function[20] $E^*(T^*)$ is nearly independent of temperature for $T^* \geq 1$ and the high-temperature Γ_2 data and lines approach T^{*2} temperature dependences (indicated by the dashed line) above 80 K. For $T^* \leq 0.02$ the quantity E is proportional to T^{*5} and Γ_2 is proportional to T^{*7}, as also is evident by comparison with the dashed line at the lower left in Fig. 15. The a-Si Γ_2 computed data points in Fig. 15 have not involved any assumptions about the characteristic temperature Θ_c. The results, however, can be fitted very well by Eq. (11) with $\Theta_c = 40 \pm 5$ K (e.g., cf. Figs. 12 and 14). There may, in fact, be significant variations in Θ_c among some other s-Si samples. That is a topic for further investigation. Experiments currently are under way to determine Θ_c for dilute p-D_2 in solid argon.

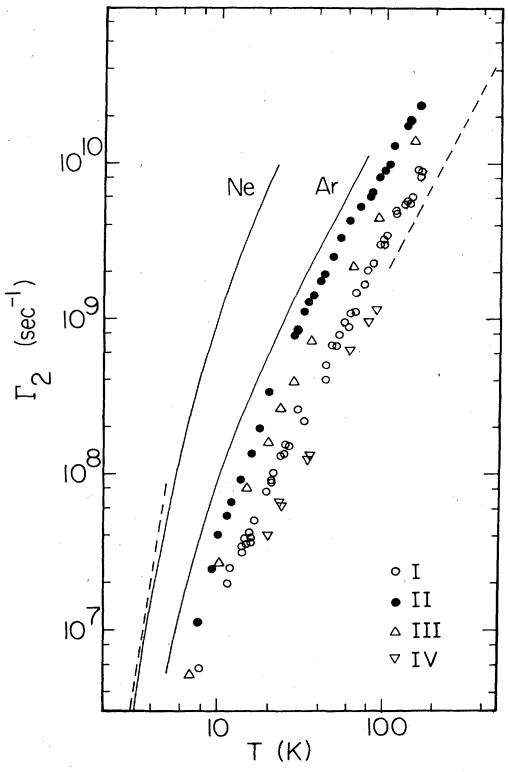

FIG. 15. Molecular correlation frequency Γ_2 for a-Si:(D,H) samples I, II, III, and IV calculated from $T_{1\alpha}$(D) and $T_{1\alpha}$(H) data. The curved lines represent Γ_2 for ortho-H_2 in solid neon and argon for comparison. The straight dashed lines show the anticipated limiting T^2 and T^7 behavior expected for a phonon-Raman process.

There is an evident chemical trend in the sample dependence of the molecular Γ_2 data plotted in Fig. 15 and reported earlier.[1,23] The Γ_2 curves systematically shift downward [i.e., C decreases in Eq. (11)] as one progresses towards host materials with larger polarizabilities. Taking ionization potential as an inverse measure of polarizability, Fig. 16 shows the trend in a semilogarithmic plot of the fitted coefficient C as a function of host ionization potential, for hydrogen relaxation data[23] in solid neon, argon, p-H_2, krypton, and the five a-Si samples discussed here. There is, in addition, an apparent distribution among the Γ_2 results for the a-Si samples (Figs. 15 and 16). Samples deposited more slowly at lower power densities appear to show larger coefficients C and thus more effective coupling between phonons and the relaxation-center molecular H_2 and D_2 electronic distributions.

If the deduced $\Gamma_2(T)$ results of Fig. 15 are correct at low temperatures then the $\Gamma_2(T)$ extend down to 10^7 sec^{-1}, that is to about $\omega_0/100$. In such a case there is very little effective EQQ interaction among the o-H_2 or the p-D_2 in molecules responsible for the low-temperature $T_{1\alpha}$(H) and $T_{1\alpha}$(D). Thus the molecular hydrogen which relaxes the bulk H and D spins must occur[3] in small microvoids or adsorbed on the surfaces of larger voids. In either case spatially-varying large static efg can quench the EQQ interactions between adjacent molecules and permit rapid nuclear relaxation times $T_1(H_2)$ and $T_1(D_2)$. Thus the number of molecules which can be effective centers of nuclear relaxation for bulk H and D is limited by the microvoid geometry.

3. *Spin diffusion*

The spin-diffusion coefficients D_H and D_D in Table III have been determined by using Eqs. (16) and (17), the fitted bottleneck relaxation times, and the determined

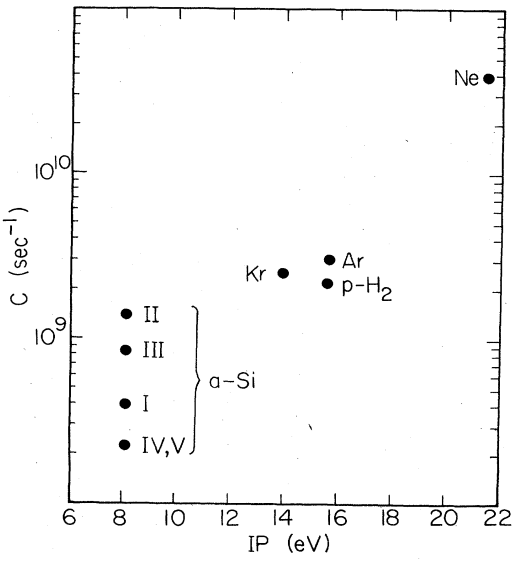

FIG. 16. The molecular correlation frequency coupling constant C obtained from $\Gamma_2 = CE^*(T^*)T^{*2}$ is plotted versus first ionization potential for the various hosts (Ne, Ar, Kr, para-H_2, a-Si).

molecular concentrations $n(H_2)$ and $n(D_2)$. The near-neighbor distances b_H and b_D were taken to be 4 Å and the average density of a-Si to be 5×10^{22} cm^{-3}. A direct comparison of results can be made only in sample I, where the ratio of tabulated spin-diffusion coefficients is

$$D_H/D_D=28/1.1=25 . \quad (23)$$

This is in fortuitously good agreement with the anticipated ratio

$$D_H/D_D=\sqrt{3/8}\gamma_H^2/\gamma_D^2=26.0 \quad (24)$$

calculated[1] on the assumptions that there are no quadrupolar interference effects on D_D for the primarily motionally-narrowed nondoublet fraction and that there is sufficient clustering of H and D that the concentrations $n(H)$ and $n(D)$ do not enter the ratio, Eq. (24).

In samples II, IV, and V the central portion of the deuteron resonance is primarily the broad central (BC) component. The bulk D_2 narrow central (NC) component so apparent in sample I is numerically insignificant in the other a-Si samples. In the broad central components spin diffusion may be much reduced by quadrupole interactions.

Consider a set of spins with a distribution of quadrupolar-induced inhomogeneous splittings characterized by a frequency ω_q and nearest-neighbor dipolar interactions characterized by a frequency ω_d. If $\omega_q \gg \omega_d$ then the spins cannot support spin diffusion as it is normally understood. This can be seen, for example, from energy conservation. If two neighboring spins mutually flip their spins, the associated energy mismatch is greater than the energy which the dipolar interaction can supply. However, this does not mean that the spin relaxation of a D to a D_2 relaxation center cannot be aided by intermediary spins.

A spin at a distance r_i from a relaxation center is connected to that relaxation center by matrix elements of order $\hbar\omega_d(r_i)$, where $\omega_d(r_i)$ characterizes the strength of the dipolar interaction between the spin and the relaxing center. Since that interaction goes as r_i^{-3}, it is not very effective in relaxing remote spins. However, the spin in question can also be coupled to the relaxing center via a number of intermediary spins. Each coupling will be of order (ω_d/ω_q) and thus a coupling via n spins will be of order $(\omega_d/\omega_q)^n$. Although this mechanism is much weaker than true spin diffusion, it can be effective for a few nearest neighbors.

There is an apparent inconsistency among the spin-diffusion coefficients listed in Table III. With the exception of sample I (which is atypical in that there is a large D_2-related narrow central component), the tabulated D_H and D_D are about the same magnitude. On the other hand, Eq. (24) predicts that in the absence of quadrupole interactions D_H should be 26 times larger than D_D under similar circumstances. If there are appreciable quadrupolar effects, D_D may be very much reduced, but that is not characteristic of the results in Table III.

However, some of the bottleneck terms may be systematically too large. It is probable that in a number of a-Si samples there is a significant distribution[3] of EQQ interaction strengths among H_2 or D_2 molecules in the microvoids. It then follows that there is a distribution of EQQ-related molecular relaxation rates Γ_Q and thus a distribution of total molecular relaxation rates

$$\Gamma=\Gamma_2+\Gamma_Q . \quad (25)$$

For $\Gamma_Q \gg \omega_0$ there would be no $T_1(H_2)$ or $T_1(D_2)$ minimum and no effective relaxation of nearby H and D. For $\Gamma_Q \leq \omega_0$ a distribution of Γ_Q would be accompanied by a broader than usual $T_1(H_2)$ or $T_1(D_2)$ minimum. The apparent Γ_2 determined from $T_{1\alpha}$ on the assumption that Γ_Q was negligible would show a frequency dependence. These are characteristic features of the proton relaxation data and analyses for samples II and III. If a significant part of the widths of the $T_{1\alpha}(H)$ minima for these samples (Fig. 12) arise from a distribution in Γ_Q, then the correct bottleneck terms B are smaller than, and the correct D_H proton spin-diffusion coefficients are larger than, the values given in Table III.

4. Relaxation by mobile carriers

Above 50 K the T_1 results (Fig. 13) for samples IV and V are different from those for the other samples described here (Fig. 11 and Ref. 1). $T_1(H)$ and both $T_1(D)$ components decrease rapidly with increasing temperature and $T_1(H)$ shows a minimum near 380 K. The 92-MHz minimum $T_1(H)$ is less than 0.2 sec and represents much too rapid a relaxation to arise from proton diffusion in the dilute proton samples IV and V. The warm-sample T_1 minimum probably arises from interaction with electron magnetic moments, either mobile carriers, or fixed paramagnetic centers. The data permit a choice between these alternatives.

If the relaxation reflects nuclear-electron contact interaction with mobile carriers, then one expects the ratio

$$\frac{T_1(D)}{T_1(H)}=\left[\frac{\gamma(H)}{\gamma(D)}\right]^2=42.44 . \quad (26)$$

In Fig. 13 a solid line has been drawn through the 92.5-MHz $T_1(H)$ data for sample V. The upper solid line is 42.44 times the lower $T_1(H)$ line and is in excellent agreement with the doublet $T_1(D)$ data for sample V. Now, for a semiconducting sample one expects

$$1/T_1 \propto \gamma^2 N\sqrt{T} , \quad (27)$$

where the number of carriers, N, may be exponentially thermally activated. Equation (27) applied to the data of Fig. 13 yields an activation energy of 37 meV.

If the $T_1(H)$ and doublet $T_1(D)$ relaxations in Fig. 13 are spin-diffusion limited and arise from spin-diffusion to the same fixed paramagnetic relaxation centers, then it follows that

$$\frac{T_1(D)}{T_1(H)}=\frac{D_H}{D_D}\left[\frac{\gamma_H\nu_D}{\gamma_D\nu_H}\right]^{1/2} . \quad (28)$$

The D_H/D_D ratio is uncertain for sample V, but the data of Fig. 13 do not show the $\nu^{1/2}$ frequency dependence of Eq. (28). There is little frequency dependence in the low-temperature $T_1(H)$ data and the room-temperature

T_1(H) is closely proportional to ν(H). It is probable that the low- and high-temperature relaxations reflect different mechanisms with the low-temperature relaxation arising from a $T_{1\beta}$ dangling bond term and the room-temperature relaxation associated with a contact interaction with mobile carriers.

IV. DISCUSSION AND CONCLUSIONS

The present NMR measurements show that there are three distinguishable components of the quadrupole broadened deuteron resonance in *a*-Si. The resolved doublet, broad central, and narrow central components must correspond to distinct bonding configurations. A principal conclusion of the present work is that there is not a one-to-one correlation between the quadrupolar line-shape components and proton or deuteron clustering, as reflected in the narrow and broad dipolar lines.

The deuteron line shape in sample I (Fig. 1), the first *a*-Si:D sample studied by DMR, showed[1] principally a well-resolved low-asymmetry quadrupolar doublet (RD) and a motionally narrowed central line (NC). The resonance has a certain resemblance to those reported[24] in many observations on predeuterated polymers between 300 and 400 K, where a doublet arises from crystalline regions and a motionally-narrowed line from the more mobile amorphous fractions. However, the present results on *a*-Si samples II, IV, and V show that the motionally-narrowed DMR component (NC) usually is a minor fraction of the observed line shape. The typical *a*-Si:D,H sample has a DMR signal which consists primarily of the doublet RD and a temperature-independent broad central line (BC), which relaxes via effectively dilute molecular D_2 relaxation centers while the RD fraction does not so relax. Upon reexamination the BC fraction also is present in the sample-I DMR spectrum.

The quadrupolar broad central DMR fraction occurs between 1 and 4 at. % in all the deuterated samples studied. The resolved doublet fraction ranges more widely, from 7 to 20 at. %. The dipolar decay comparisons of Sec. III B show that the resolved doublet and the broad central components both contain more and less clustered deuteron fractions. However the FTDMR-QE spectrum (Fig. 9) for an echo at large 2τ (1200 μsec) has a more singular (RD) doublet and a diminished (BC) central fraction. Thus the broad central (BC) component corresponds to a more-clustered deuteron configuration than does the well-defined part of the resolved doublet (RD). There also may be some motional loss of quadrupolar order on a scale of 1 msec, even at 6 K.

Both RD and BC are broadened by quadrupole interactions. Their spin magnetizations cannot migrate by flip-flop spin diffusion over extended distances. However, their magnetizations can migrate over shorter distances, of the order of two or three lattice separations. We conclude that in order for BC to relax efficiently to D_2 molecules, it is necessary that the BC deuterons be located close to those D_2 molecules which serve as relaxation centers. That is the BC deuterons must be located close to void surfaces. The obvious candidates for inclusion in the broad central signal fraction thus include those deuterons which are chemisorbed onto microscopically rough surfaces of microvoids, and also the deuterons in the first few *a*-Si layers surrounding these microvoids. For both these deuteron configurations the quadrupolar spectrum can be much averaged and represents a distribution of Si-D configurations and corresponding distributions of η and ν_q. In this sense the broad central fraction corresponds to small ν_q and weakly bound deuterium (WBD). The first few Si layers around a rough microvoid contain local configurations of great potential strain and disorder. The hydrogen will cluster preferentially in such disordered regions. We propose that the DMR broad central (BC) fraction arises from these deuterons clustered in disordered regions near microvoids and thus near the molecular D_2 relaxation centers, which are the D_2 in small voids or near the surfaces of larger voids. Since there are more microvoids in the less-dense regions of the *a*-Si it follows that there is more of the central (BC) fraction in such regions. The limited 1-to-4—at. % range observed for the broad central fraction represents the limited disordered volume near the *p*-D_2 relaxation centers in small microvoids or on rough void surfaces. We plan to make further investigations of the broad central (BC) component by using spectral hole-burning, proton decoupling, and three-pulse deuteron spin-alignment sequences.

The resolved doublet (RD) DMR signal corresponds primarily to well-defined SiD and SiD_2 configurations located in less-disordered lattice environments. The slow dipolar damping shows that the best-defined (RD) configurations contain less clustered deuterons than do the broad central (BC) configurations. The smaller clustering and the well-resolved 66-kHz quadrupolar doublet reduce the spin-diffusion for the doublet (RD) fraction, but it remains likely that the RD deuterons are located well-removed from those *p*-D_2 molecules which serve as rapid relaxation centers for the other fractions. The resolved doublet (RD) fraction has a long spin-lattice relaxation time which is not related to the $T_1(D_2)$ of the deuterons in the *p*-D_2 relaxation centers.

The DMR resonance line from the motionally-narrowed central (NC) component corresponds to a spin fraction with homogeneous broadening, a spin temperature, and which relaxes efficiently to the low EQQ void surface *p*-D_2 relaxation centers. The NC fraction usually is small and probably arises from *p*-D_2 (and perhaps *o*-D_2) molecules[25] in dense fluid and solid D_2 in the bulk volume of larger voids. The molecules have long intrinsic relaxation times and are relaxed[3] by the surface-dominated effectively dilute *p*-D_2 relaxation centers. Sample I, which has the largest NC fraction (1.5 at. %) of the samples studied, was prepared (from a 95% D_2 starting gas) on a room-temperature substrate and at large rf power level. The sample presumably has a columnar structure with large void volumes in the less crystalline intercolumnar regions. Higher-quality samples made at lower power levels (sample II) and at 230 °C substrate temperature (sample V) have much less of the narrow central (NC) component and much less D_2.

Low-temperature T_1 minima observed for protons and deuterons in *a*-Si have been shown to arise from relaxation via effectively dilute molecular *o*-H_2 and *p*-D_2. The

relaxation-center molecular concentrations needed to account for the T_1 minima range from a few ppm to nearly 1000 ppm. In order for the molecules to serve as effective relaxation centers, they must have an EQQ interaction no more than about 10^{-5} that of normal solid and liquid H_2 or D_2. That is to say, it is probable[3] that the relaxation-center molecules occupy small voids or are adsorbed on void surfaces. These molecules are deduced to have molecular correlation frequencies whose temperature dependence is the T^2 to T^7 power-law characteristic of a phonon-Raman process. In some samples the molecular correlation frequencies deduced below 50 K indicate the presence of a wide distribution of intermolecular EQQ interactions. The magnitude of Γ_2 in various hosts varies with the polarizability and also varies by an order of magnitude among the a-Si samples studied.

The H and D NMR results described here show no evidence for the presence of a proposed[26] "three-center bond" configuration in which an H_2 or D_2 molecule is located between two Si atoms whose bond otherwise would be strained or broken. It is not clear whether H_2 and D_2 in the proposed configuration would be free to rotate about the line connecting the two Si atoms. However, even if rotation were to occur, the configuration cannot act as a relaxation center for H or D.

Assume that an H_2 in the four-center configuration were free to rotate about the Si-Si axis. The H_2 then acts as a rigid rotator with energies given by

$$E(j)=E_0 j^2 \sin^2\theta \ , \tag{29}$$

where j takes on integral values and θ is the angle between the H_2 axis and the line connecting the two Si atoms. Since there is only one rotational degree of freedom (and not two, as is usually the case for H_2 rotation), there is no analog to the usual states of different m_J within the J manifold for free H_2. The spin relaxation of the H_2 nuclear spin depends upon the H_2 molecule making transitions between states of different m_J. Since neither these transitions nor any analog of them exists in the proposed three-center configuration, such H_2 could only relax slowly and cannot act as relaxation centers for lattice H (unless $\Delta J=2$ transitions occur, since $J=\pm 1$ have the same energy and relaxation could occur).

ACKNOWLEDGMENTS

We have benefited from stimulating conversations with R. Fisch and M. S. Conradi. This work was supported in part by the Low Temperature Physics Program of the National Science Foundation (NSF) Division of Materials Research under Grants Nos. DMR-82-04166 and DMR-83-04473. One of us (D.J.L.) has benefited from a Xerox Corporation grant and a Harvard University Research grant.

*Present address: McDonnell Douglas Research Laboratories, St. Louis, MO 63166.

[1]D. J. Leopold, J. B. Boyce, P. A. Fedders, and R. E. Norberg, Phys. Rev. B **26**, 6053 (1982).

[2]D. J. Leopold, B. S. Coughlan, P. A. Fedders, R. E. Norberg, J. B. Boyce, and J. C. Knights, J. Non-Cryst. Solids **66**, 121 (1984).

[3]P. A. Fedders, R. Fisch, and R. E. Norberg, Phys. Rev. B (to be published).

[4]H. V. Löhneysen, H. J. Schink, and W. Beyer, Phys. Rev. Lett. **52**, 549 (1984).

[5]J. E. Graebner, B. Golding, L. C. Allen, D. K. Biegelsen, and M. Stutzmann, Phys. Rev. Lett. **52**, 553 (1984).

[6]J. E. Graebner, L. C. Allen, and B. Golding, Phys. Rev. B **31**, 904 (1985).

[7]Y. J. Chabal and C. K. N. Patel, Phys. Rev. Lett. **53**, 210 (1984).

[8]R. A. Street, J. C. Knights, and D. K. Biegelsen, Phys. Rev. B **18**, 1880 (1978).

[9]M. Mokarram and J. L. Ragle, J. Chem. Phys. **59**, 2770 (1973).

[10]J. C. Knights and G. Lucovsky, in *Critical Reviews in Solid State and Materials Sciences,* edited by D. E. Schuele and R. W. Hoffman (Chemical Rubber Co., Boca Raton, Fla., 1980), Vol. 9, p. 210; E. C. Freeman and William Paul, Phys. Rev. B **18**, 4288 (1978).

[11]J. A. Reimer, R. W. Vaughan, and J. C. Knights, Phys. Rev. B **24**, 3360 (1981).

[12]W. E. Carlos and P. C. Taylor, Phys. Rev. B **26**, 3605 (1982).

[13]A. Abragam and J. Winter, C. R. Acad. Sci. **249**, 1633 (1959).

[14]N. Boden, S. M. Hanlon, Y. K. Levine, and M. Mortimer, Chem. Phys. Lett. **57**, 151 (1978).

[15]M. S. Conradi and R. E. Norberg, Phys. Rev. B **24**, 2285 (1981).

[16]W. E. Carlos, P. C. Taylor, S. Oguz, and W. Paul, in *Tetrahedrally Bonded Amorphous Semiconductors (Carefree, Arizona),* edited by R. A. Street, D. K. Biegelsen, and J. C. Knights (AIP, New York, 1981), p. 67.

[17]P. A. Fedders, Phys. Rev. B **30**, 3603 (1984).

[18]P. A. Fedders, Phys. Rev. B **20**, 2588 (1979).

[19]N. F. Ramsey, *Molecular Beams* (Oxford University Press, London, 1956), p. 235.

[20]J. Van Kranendonk, Physica (Utrecht) **20**, 871 (1954).

[21]J. Van Kranendonk and M. B. Walker, Can. J. Phys. **46**, 2441 (1968).

[22]R. E. Norberg, Phys. Rev. B (to be published).

[23]M. S. Conradi, K. Luszczynski, and R. E. Norberg, Phys. Rev. B **20**, 2594 (1979).

[24]H. W. Spiess, *Advances in Polymer Science,* edited by H. H. Kausch and H. G. Zachmann (Springer, Berlin, 1984).

[25]B. Maraviglia, F. Weinhaus, S. M. Myers, and H. Meyer, in *Proceedings of the 12th International Conference on Low Temperature Physics, Kyoto, 1970,* edited by Eizo Kanda (Academic, Kyoto, 1971).

[26]M. E. Eberhart, K. H. Johnson, and D. Adler, Phys. Rev. B **26**, 3138 (1982).